Single-Atom Catalysis

How to cite: *Angew. Chem. Int. Ed.* **2021**, *60*, 26054–26062
International Edition: doi.org/10.1002/anie.202108585
German Edition: doi.org/10.1002/ange.202108585

Tailoring the Local Environment of Platinum in Single-Atom Pt_1/CeO_2 Catalysts for Robust Low-Temperature CO Oxidation

Dong Jiang, Yonggang Yao, Tangyuan Li, Gang Wan, Xavier Isidro Pereira-Hernández, Yubing Lu, Jinshu Tian, Konstantin Khivantsev, Mark H. Engelhard, Chengjun Sun, Carlos E. García-Vargas, Adam S. Hoffman, Simon R. Bare, Abhaya K. Datye, Liangbing Hu,* and Yong Wang**

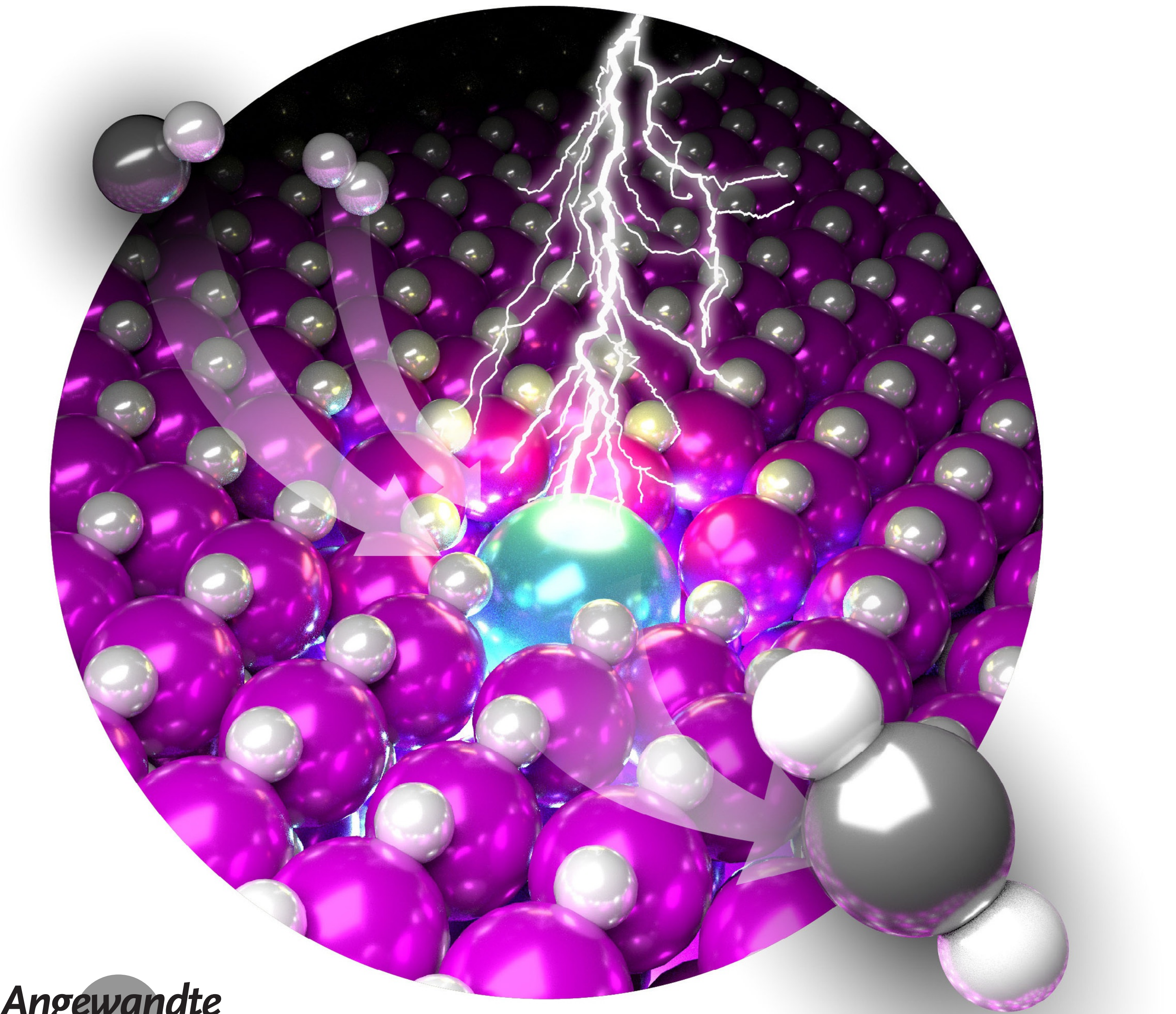

Abstract: *A single-atom Pt_1/CeO_2 catalyst formed by atom trapping (AT, 800 °C in air) shows excellent thermal stability but is inactive for CO oxidation at low temperatures owing to over-stabilization of Pt^{2+} in a highly symmetric square-planar Pt_1O_4 coordination environment. Reductive activation to form Pt nanoparticles (NPs) results in enhanced activity; however, the NPs are easily oxidized, leading to drastic activity loss. Herein we show that tailoring the local environment of isolated Pt^{2+} by thermal-shock (TS) synthesis leads to a highly active and thermally stable Pt_1/CeO_2 catalyst. Ultrafast shockwaves (>1200 °C) in an inert atmosphere induced surface reconstruction of CeO_2 to generate Pt single atoms in an asymmetric Pt_1O_4 configuration. Owing to this unique coordination, $Pt_1^{\delta+}$ in a partially reduced state dynamically evolves during CO oxidation, resulting in exceptional low-temperature performance. CO oxidation reactivity on the Pt_1/CeO_2_TS catalyst was retained under oxidizing conditions.*

Introduction

Supported precious metals with atomic dispersion have proved promising for achieving maximum atom efficiency as well as improved activity and selectivity in catalyzing a growing number of thermo-, electro-, and photo-driven chemical reactions.[1] A major challenge for single atom catalysts (SACs) in future industrial applications is attaining high reactivity while simultaneously demonstrating high thermal stability.

CO oxidation is industrially important in vehicle emission control, requiring catalysts with high reactivity (high concentrations of active sites) as well as thermal stability.[2] Single-atom Pt_1/CeO_2 has been widely studied for emission control applications.[1a,3] To achieve high thermal stability at high metal loadings (≥1 wt%), Pt atoms need to form strong covalent bonds with the support.[1a,3a,4] For instance, we developed an atom trapping (AT) method, i.e., heat treatment at 800 °C in air,[1a] allowing volatile PtO_2 to be trapped at the most thermodynamically stable binding sites, e.g., monoatomic CeO_2 (111) step edges.[3a,b] Using this approach, we recently reported the synthesis of thermally stable Pt_1/CeO_2 catalysts at Pt loadings of up to 3 wt%.[3a] In these catalysts, Pt adopts a highly symmetric square-planar Pt_1O_4 coordination, which can be expected from the crystal field theory for a Pt^{2+} d^8 electronic configuration.[3g,5] Such an over-stabilization results in a greatly compromised ability of isolated Pt^{2+} for activating gas-phase molecules (e.g., CO, H_2),[5b,6] making them nearly inactive for CO oxidation below 200 °C.[1a,7] A common feature of these strongly bonded Pt single atoms is that they require some form of activation (e.g., reduction in CO/H_2, or treatment in steam) to achieve enhanced low temperature CO oxidation performance.[3c–e,7,8] The highest activity is obtained when ionic Pt single atoms are transformed into metallic clusters/NPs.[3e,7,8b] However, when exposed to oxidizing conditions at elevated temperatures, Pt clusters/NPs break up into single atoms that revert to a low activity state.[3e,7] This is much less desirable for the application of these SACs in emission control systems, especially during the cold-start of engines. Hence, there is an urgent need to develop single-atom Pt_1/CeO_2 catalysts that demonstrate CO oxidation activity at low temperatures, and at the same time are resistant to the activity loss under oxidizing conditions.

The distinct behavior of single atoms from that of NPs stems from the unique local coordination environment of isolated metal atoms, as well as their interactions with the support.[9] Therefore, insights into the coordination and electronic states of supported single atoms as well as their dynamic changes under reaction conditions are crucial for unraveling the precise structure–function relationships of SACs.[3h,10] For example, DeRita et al. demonstrated that under varied redox conditions isolated Pt on TiO_2 can adopt a range of local coordination and oxidation states, showing a strong influence on CO oxidation reactivity.[10c] Similarly, Tang et al. confirmed that Rh single atoms adapt their local coordination under various redox conditions, including calcination in O_2, reduction in H_2, and reverse water gas shift (RWGS) reaction.[10d] To achieve high thermal stability, these authors used very low loadings of metals (0.025–0.05 wt%) so

[*] Dr. D. Jiang, Dr. X. I. Pereira-Hernández, C. E. García-Vargas, Prof. Y. Wang
The Gene and Linda Voiland School of Chemical Engineering and Bioengineering, Washington State University
Pullman, WA 99164 (USA)
E-mail: yong.wang@pnnl.gov

Dr. Y. G. Yao, T. Y. Li, Prof. L. B. Hu
Department of Materials Science and Engineering
University of Maryland
College Park, MD 20742 (USA)
E-mail: binghu@umd.edu

Dr. Y. G. Yao
Current address: State Key Laboratory of Materials Processing and Die & Mould Technology
School of Materials Science and Engineering
Huazhong University of Science and Technology
Wuhan, 430074 (China)

Dr. G. Wan, Dr. A. S. Hoffman, Dr. S. R. Bare
Stanford Synchrotron Radiation Lightsource
SLAC National Accelerator Laboratory
Menlo Park, CA 94025 (USA)

Dr. Y. B. Lu, Dr. J. S. Tian, Dr. K. Khivantsev, Dr. M. H. Engelhard, Prof. Y. Wang
Institute for Integrated Catalysis
Pacific Northwest National Laboratory
Richland, WA 99354 (USA)

Dr. C. J. Sun
X-ray Science Division, Advanced Photon Source
Argonne National Laboratory
Lemont, IL 60439 (USA)

Prof. A. K. Datye
Department of Chemical and Biological Engineering and Center for Micro-Engineered Materials, University of New Mexico
Albuquerque, NM 87131 (USA)
E-mail: datye@unm.edu

Supporting information and the ORCID identification number(s) for the author(s) of this article can be found under: https://doi.org/10.1002/anie.202108585.

that agglomeration of isolated metal atoms could be avoided.[3g,9a,10c]

Here we demonstrate single-atom Pt_1/CeO_2 catalyst at an industrially relevant loading (1 wt%) that is oxidation resistant and reactive for low-temperature CO oxidation can be achieved by tailoring the local environment of isolated Pt sites. In particular, single-atom Pt_1/CeO_2 was synthesized by a thermal-shock (TS) method to tailor the Pt–CeO_2 interaction, i.e., the local coordination and electronic states of isolated Pt on CeO_2. The TS synthesis has been developed for stabilizing high-entropy-alloy NPs as well as metal single atoms on different supports (e.g., carbon, C_3N_4, and TiO_2).[11] Here, controlled high-temperature (>1200 °C) shockwaves are produced by periodic on–off heating that consists of a short on-state (ca. 500 ms) and a six-times longer off-state (Figure S1). The high-temperature flash heating drives Pt dispersion by restructuring the CeO_2 surface and making it suitable for forming strong Pt–O–Ce bonding, while the rapid cooling (ca. 10^4 K s^{-1}) off-state prevents the sintering of Pt and CeO_2. Furthermore, by performing TS in an inert atmosphere, vapor-phase transport of PtO_2 is largely limited, allowing Pt atoms to be stabilized at sites different from the most thermodynamically stable square-planar pockets at CeO_2 step edges. As a result, stable Pt^{2+} single atoms in an asymmetric Pt_1O_4 configuration are formed (Figure 1 a). Originating from such asymmetric local coordination, partially reduced $Pt_1^{\delta+}$ species in Pt_1O_{4-x} configurations are induced during CO oxidation, leading to a significantly superior low-temperature activity compared to Pt_1/CeO_2 synthesized via atom trapping (AT).

Results and Discussion

As illustrated in Figure 1 a, tetraammineplatinum nitrate (TAPN) as the Pt precursor was introduced onto CeO_2 by incipient wetness impregnation (IWI), followed by AT and TS treatments to obtain the Pt_1/CeO_2_AT and Pt_1/CeO_2_TS catalysts with 1 wt% Pt loading, respectively. The absence of X-ray diffraction for Pt/PtO_2 (Figure S2) indicates the high dispersion of Pt on CeO_2. Atomic dispersion of Pt was confirmed by aberration-corrected scanning transmission electron microscopy (AC-STEM) in the high-angle annular dark-field (HAADF) imaging mode, where only isolated Pt atoms can be observed in both catalysts (Figure 1 b,c). Since the two methods employed the same precursor (i.e., TAPN deposited on polyhedral CeO_2 obtained by calcination of cerium nitrate), both Pt_1/CeO_2 catalysts present multiple nanofacets (e.g., {111}, {110}, and {100}) without noticeable difference (Figures S3 and S4). The BET surface areas were measured to be 40.0 m^2 g^{-1} for Pt_1/CeO_2_AT and 67.1 m^2 g^{-1} for Pt_1/CeO_2_TS (Table S1). Compared to atom trapping, which requires prolonged heating at 800 °C, the ultrafast pulse heating and cooling helps preserve the surface area of the CeO_2 support (Figure 1 a).[11a,b] In addition, this thermal-shock method shows much superior cost-effectiveness to conventional furnace calcination in terms of the energy and time spent for catalyst preparation (Table S2).

The single-atom nature of supported Pt was further investigated by X-ray absorption spectroscopy (XAS) at Pt L_3-edge which provides information on the oxidation state and the local coordination environment of Pt.[3a,4a,12] Figure 1 d shows the X-ray absorption near edge structure (XANES) spectra of Pt foil and as-synthesized Pt_1/CeO_2 catalysts in an air-exposed state. The white line intensity of Pt_1/CeO_2_TS is much higher than that of Pt foil but is close to that of Pt_1/CeO_2_AT which has been proven to exclusively contain isolated and ionic Pt species in a mixed +2/+4 charge state (Pt^{2+} is dominant).[3a,7] Given the absence of Pt–Pt scattering as clearly indicated in the extended X-ray absorption fine structure (EXAFS), the as-synthesized Pt_1/CeO_2_TS is also dominated by isolated Pt^{2+} cations (Figure 1 e). This is also confirmed by X-ray photoelectron spectroscopy (XPS) in the Pt 4f region (Figure S5a). It should be noted that compared to Pt_1/CeO_2_AT, Pt_1/CeO_2_TS shows a slightly lower white line intensity (Figure 1 d), suggesting a slightly more reduced valence state or coordination symmetry of ionic Pt^{2+}.[13] More importantly, there appears a rising-edge feature above the XANES absorption edge of Pt_1/CeO_2_TS, evidenced by a bump in the first-order derivative curve (inset of Figure 1 d). Appearance of such rising edge is believed to be associated with the decreased local coordination symmetry around Pt sites.[14] This confirms our initial speculation that TS produces isolated Pt^{2+} with an asymmetric Pt_1O_4 configuration (Figure 1 a).

The local coordination environments of isolated Pt^{2+} in the two Pt_1/CeO_2 catalysts were analyzed by carefully fitting the EXAFS spectra (Figure S6). As summarized (Table 1), Pt_1/CeO_2_AT can be readily fitted with a near-perfect square-planar Pt_1O_4 configuration with four equivalent Pt−O bonds, which is preferred by Pt^{2+} as a d^8 ion.[3g,5a] For Pt_1/CeO_2_TS, employing the same high-symmetry model led to a Pt–O coordination number (CN) of approximately 3.5 (Table S3), indicating a defect Pt_1O_3 motif. This is not reasonable for the air-exposed state, since it has been proposed that excess Pt−O bonds will form from ambient O_2 once there is a vacancy (O_V), resulting in a CN > 4.[3a,10e] Instead, improved fitting results were obtained from an asymmetric square-planar Pt_1O_4 geometry with three shorter Pt–O_S distances of 1.979 Å and one longer Pt–O_L distance of 2.051 Å, which most likely involves surface hydroxy groups (-OH) or chemisorbed O* as suggested by the O 1s XPS results (Figure S5b). A similar structure has been proposed for isolated Pt^{2+} ontop anatase TiO_2 due to its tetragonal crystalline structure,[3g,9a] which can be expected here considering the binding sites created by the TS-induced surface reconstruction of CeO_2. Therefore, based on above combined XANES (Figure 1 d) and EXAFS (Figure 1 e) analysis, compared to AT that produced a near-perfect square-planar Pt_1O_4 coordination, an asymmetric Pt_1O_4 geometry was formed by the TS treatment. This further confirms our initial hypothesis (Figure 1 a) and suggests that isolated Pt formed by TS is located in a different surface site of CeO_2 compared to that prepared by AT.

The effect of such asymmetric Pt_1O_4 coordination on low-temperature CO oxidation was evaluated under O_2-rich conditions. As shown in Figure 2 a, Pt_1/CeO_2_AT was inactive below about 200 °C and showed better activity than bare

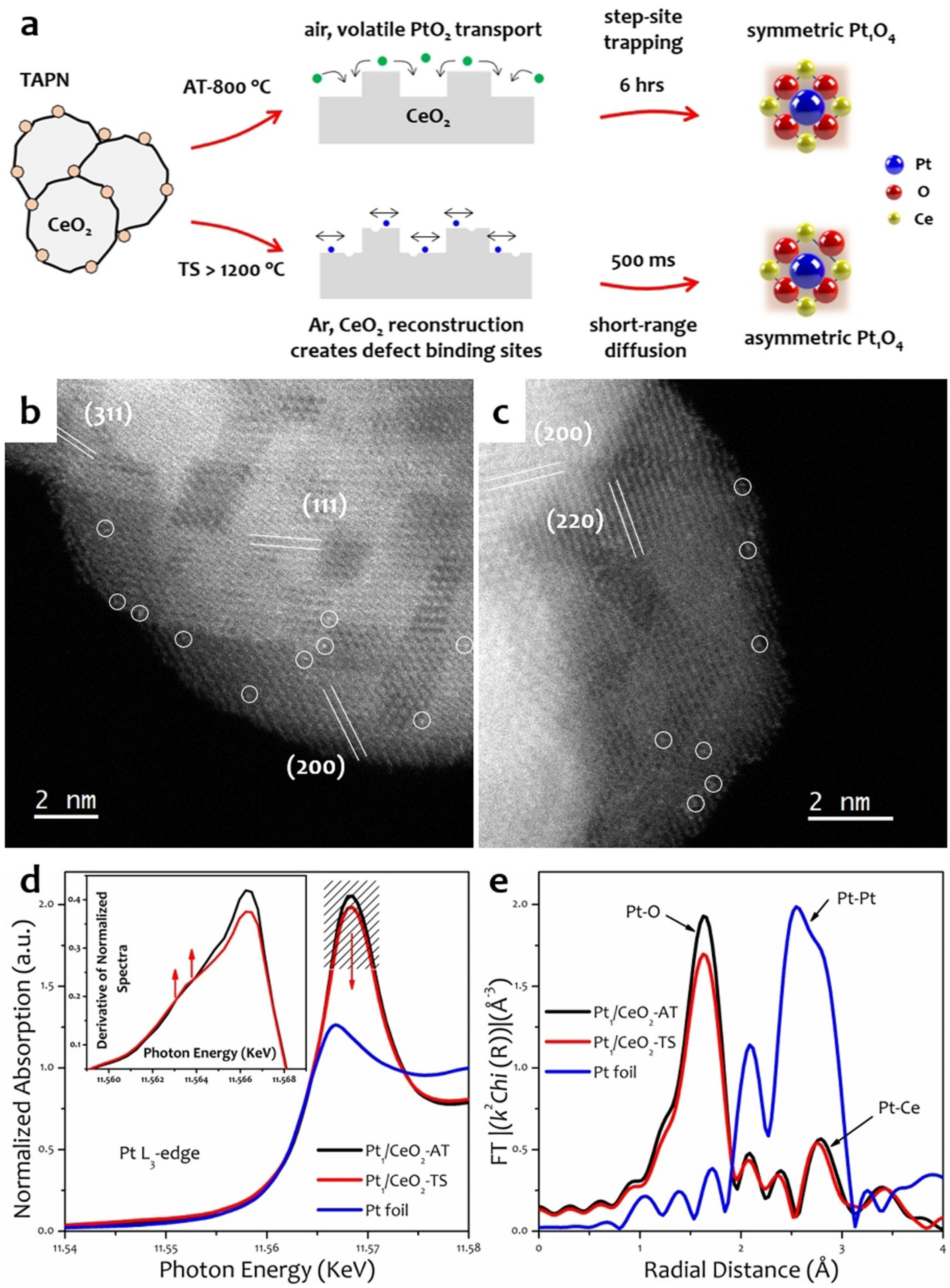

Figure 1. a) AT and TS synthesis of single-atom 1 wt% Pt_1/CeO_2 catalysts showing the symmetric (near-perfect) and asymmetric (distorted square-planar) Pt_1O_4 coordination in Pt_1/CeO_2_AT and Pt_1/CeO_2_TS, respectively. b, c) AC-STEM images of as-synthesized Pt_1/CeO_2_AT (b) and Pt_1/CeO_2_TS (c) showing the exclusive presence of isolated Pt atoms. d) Pt L_3-edge XANES and e) Fourier transform of k^2-weighted EXAFS of as-synthesized Pt_1/CeO_2 catalysts and the Pt foil reference. Inset of (d) is the first derivative of the normalized XANES in (d).

CeO_2 only at temperatures above about 240 °C, which is similar to previous reports.[3c,7] In contrast, Pt_1/CeO_2_TS showed a significantly enhanced low-temperature activity, evidenced by a significantly lower T_{50} value (temperature required for 50% conversion of CO) of about 150 °C as compared to about 287 °C for Pt_1/CeO_2_AT (Table S4). It also showed good cycling stability as no deactivation in low-temperature CO oxidation was observed after repeated light-

Table 1: Best fitting results of EXAFS over as-synthesized Pt_1/CeO_2_AT and Pt_1/CeO_2_TS.

	Scattering pair	CN	R [Å]	σ^2 [Å^2]	R factor	Comment
Pt_1/CeO_2_AT	Pt–O	4 (fixed)	1.995	0.00119	0.0074	symmetric (near-perfect square-planar) Pt_1O_4
Pt_1/CeO_2_TS	Pt–O_S[a] Pt–O_L[b]	3 (fixed) 1 (fixed)	1.979 2.051	0.00112 0.00070	0.00592	asymmetric (distorted square-planar) Pt_1O_4

[a] O_S is a lattice oxygen atom of CeO_2 bonded to Pt with a shorter Pt–O bond length. [b] O_L is an oxygen atom at a longer distance, possibly lattice oxygen or foreign oxygen atoms from surface hydroxy groups (-OH) or chemisorbed O*.

off measurements (Figure 2a). Although the reductive treatment on Pt_1/CeO_2_AT can enhance the low-temperature performance (i.e., decreased T_{10}, T_{50}, and T_{90} in Figure 2b, right) by forming Pt NPs,[7] the so-called activated catalyst is susceptible to drastic activity loss (nearly back to the original T_{10}, T_{50}, and T_{90} in Figure 2b, right) once being oxidized at

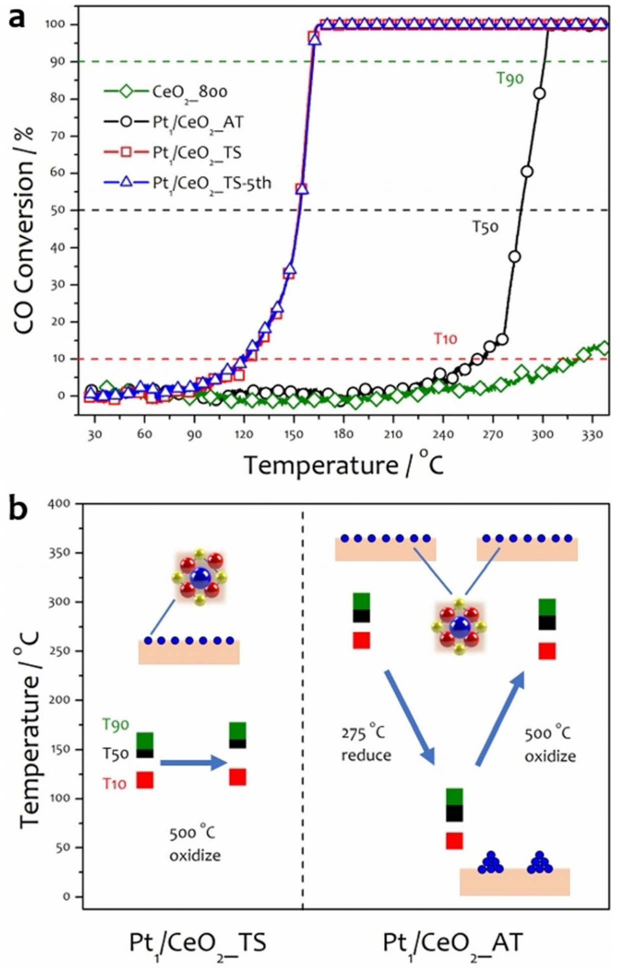

Figure 2. a) CO light-off curves collected over as-synthesized Pt_1/CeO_2_AT, Pt_1/CeO_2_TS, and bare CeO_2 calcined at 800 °C in air. Reaction conditions: 1% CO, 10% O_2, with N_2 balance, GHSV of 200 L/gh. b) The T_{10}, T_{50}, and T_{90} temperatures (temperatures required for 10%, 50%, and 90% CO conversion) of Pt_1/CeO_2 catalysts in the as-synthesized state and after reductive (at 275 °C in 5% CO for 30 min) and oxidative treatment (at 500 °C in 10% O_2 for 2 h). The dispersion status as well as the local coordination of Pt atoms at the corresponding stages are also illustrated.

temperatures >400 °C.[2d] This is consistent with previous experimental observations by Gänzler et al. that redispersion of metallic Pt NPs (<2 nm) on CeO_2 readily occurred at 400 °C in an oxidizing atmosphere.[8d] In contrast, very minor increases in T_{10}, T_{50}, and T_{90} (2–10 °C) were observed for the Pt_1/CeO_2_TS catalyst, even after being oxidized at 500 °C (Figure 2b, left).

These results clearly confirmed that enhanced low-temperature activity as well as high thermal stability can be achieved in the single-atom Pt_1/CeO_2_TS catalyst. Careful STEM investigations have excluded the morphological effect of the ceria support (Figures 1b,c, S3, and S4) from high-temperature facet reconstruction,[15] which could influence the Pt–CeO_2 interaction as well as O_2 activation during CO oxidation.[16] Such an enhanced low-temperature CO oxidation activity cannot be solely explained by the higher surface area of Pt_1/CeO_2_TS, which is only approximately 1.5 times that of Pt_1/CeO_2_AT (Table S1). Catalyst reducibility does not appear to induce such a difference, since temperature-programmed reduction in CO indicated that the surface lattice oxygen (O_O) in both catalysts can be readily removed at <90 °C (Figure S7), and in fact, Pt_1/CeO_2_AT even showed a more pronounced low-temperature reducibility possibly due to a stronger Pt–CeO_2 interaction.[7] Influence of Ce^{3+}/V_O (oxygen vacancy) that could be introduced by TS treatment in an inert atmosphere was also excluded by surface sensitive XPS. As-synthesized Pt_1/CeO_2 (AT and TS) catalysts showed similar contents of defect-related O species (7–10%) and Ce^{3+} ions (16–19%) on the surface (Figure S5b,c).[7,17]

Kinetic studies were also performed to further understand the effect of the asymmetric coordination environment of Pt^{2+} caused by TS synthesis. Although two Pt_1/CeO_2 catalysts showed similar apparent activation energies (E_a) of 60–70 kJ mol^{-1} (Figure S8), they exhibited distinct reaction orders for the reactants (Figure S9). Pt_1/CeO_2_AT showed the order of 0.76 for CO and approximately 0 for O_2, while Pt_1/CeO_2_TS showed the order of approximately 0 for both CO and O_2. A similar E_a might suggest a similar mechanism for the two catalysts, while different reaction orders for CO clearly indicate that the kinetic relevance of CO adsorption/activation has been largely weakened for Pt_1/CeO_2_TS. Therefore, it can be reasonably inferred that compared to the over-stabilized Pt^{2+} on CeO_2 via AT, the asymmetric Pt_1O_4 coordination induced by TS renders much enhanced CO activation, and thereby accelerated low-temperature CO oxidation (Figure 2a).

Diffuse reflectance infrared Fourier transform spectroscopy (DRIFTS) using CO as a probe molecule is powerful for probing the nature of supported PGM species, as well as the site evolution under reaction conditions.[1a,9,10c,e,f,12,18] Herein, after 350 °C pretreatment in 10% O_2, in situ DRIFTS was performed at different temperatures and conditions over the two Pt_1/CeO_2 catalysts, which can be divided into two consecutive stages (Figure 3a). The phase-I showed CO

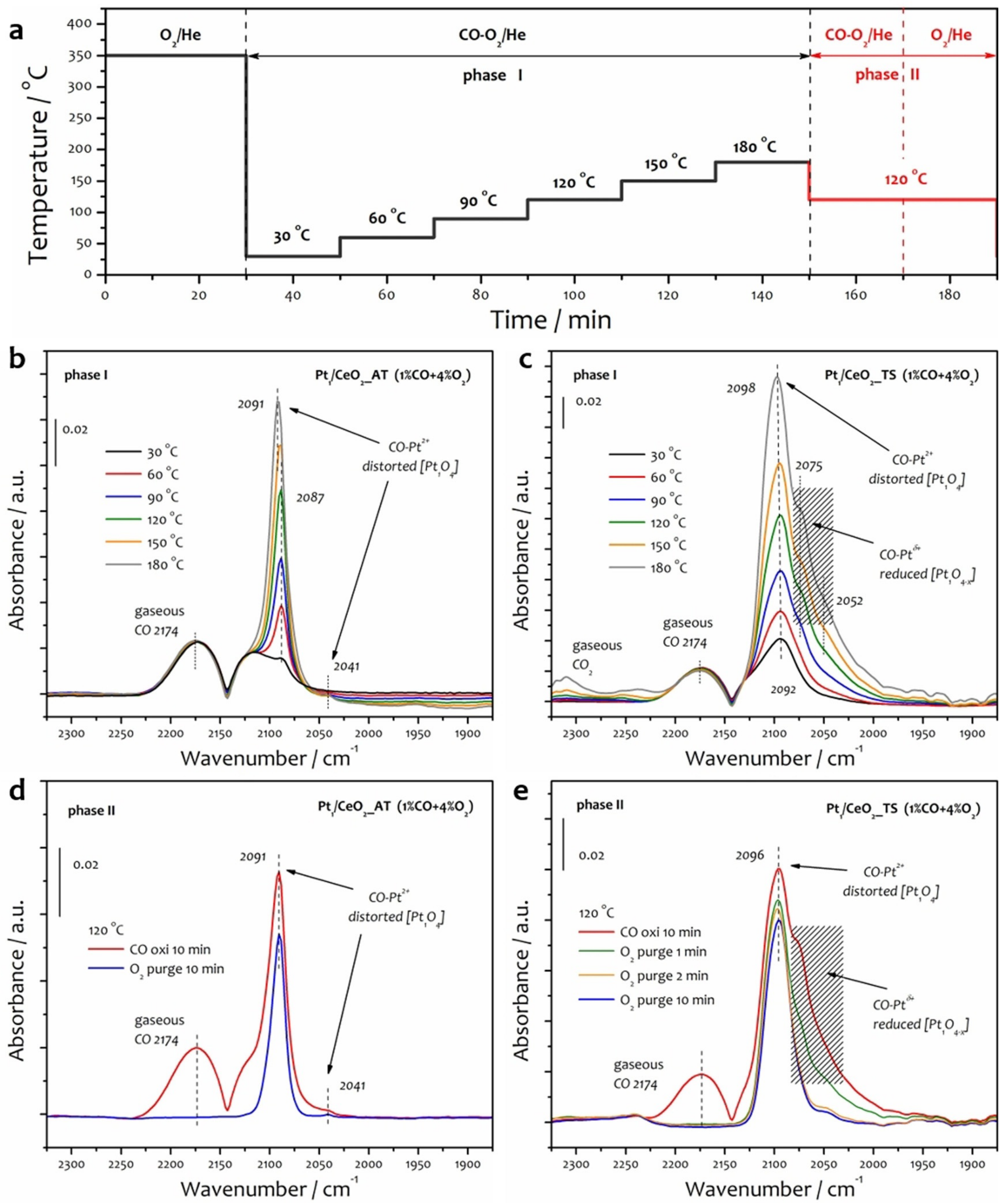

Figure 3. a) In situ diffuse reflectance infrared Fourier transform spectroscopy (DRIFTS) measurements over Pt_1/CeO_2_AT and Pt_1/CeO_2_TS catalysts under CO oxidation (1% CO, 4% O_2, He balance, 60 mL min^{-1}) and oxidizing conditions (4% O_2, He balance, 60 mL min^{-1}). Ramping rate: 20 °C min^{-1}. b, c) DRIFTS spectra recorded at different temperatures (30–180 °C) under CO oxidation in phase-I over Pt_1/CeO_2_AT (b) and Pt_1/CeO_2_TS (c) catalysts. d, e) DRIFTS recorded at 120 °C in phase-II over Pt_1/CeO_2_AT (d) and Pt_1/CeO_2_TS (e) catalysts under CO oxidation followed by purging in O_2/He.

oxidation in a temperature-programmed manner. In Figure 3b, at 30 °C, Pt_1/CeO_2_AT shows a very weak peak around 2087 cm^{-1}, which has been widely ascribed to CO linearly adsorbed on isolated Pt^{2+} cations.[1a,7,19] Here we tentatively assign this 2087 cm^{-1} peak to CO on isolated Pt^{2+} in a distorted Pt_1O_4 configuration, since both computational and surface science studies have suggested that perfect square-planar Pt_1O_4 hardly chemisorbs CO even at −150 °C.[3b,6,20] The low intensity of the 2087 cm^{-1} peak indicates that Pt^{2+} in Pt_1/CeO_2_AT presents a near-perfect square-planar Pt_1O_4 coordination environment, which is consistent with our EXAFS analysis (Figure 1e and Table 1) as well as the pulsed CO chemisorption result showing a weak CO uptake (2.6% of the amount of loaded Pt atoms) at 30 °C (Figure S10). Notably, the intensity of this CO–Pt^{2+} peak at approximately 2090 cm^{-1} increases as the temperature increases up to 180 °C (Figure 3b), suggesting a more pronounced distortion of the Pt_1O_4 configuration (an increased coordination asymmetry) under CO oxidation at elevated temperatures, which can also be traced by the slight peak shift to higher wavenumbers. Very recently, slight distortion and displacement of Pt^{2+} upon CO chemisorption was also suggested by Maurer et al. based on combined UHV-FTIRS and DRIFTS studies over a steam-treated Pt_1/CeO_2 catalyst.[3e] More intense perturbations of the local structure by CO has been observed for supported Pd in the forms of both single atoms and NPs.[10e,21]

In contrast, Pt_1/CeO_2_TS shows one symmetric while more intense CO–Pt^{2+} IR peak at a slightly higher wavenumber of 2092 cm^{-1} when flowing CO and O_2 at 30 °C (Figure 3c). This also confirms the generation of isolated Pt^{2+} with an asymmetric Pt_1O_4 geometry by the TS synthesis, in accordance with the increased CO uptake (29 % of loaded Pt atoms) at 30 °C compared to that (2.6 % of loaded Pt) for Pt_1/CeO_2_AT (Figure S10). The slightly different peak positions (2092 vs. 2087 cm^{-1}) for the two catalysts also indicate different local environments (e.g., location, coordination) of isolated Pt^{2+} that lead to different Pt–CeO_2/CO–Pt^{2+} interactions in the two catalysts. The broader peak in Pt_1/CeO_2_TS also suggests a wider distribution of local environments of Pt^{2+}, as expected for TS synthesis which involves the intense surface reconstruction of CeO_2 and limits the vapor-phase transport of PtO_2 to the most thermodynamically stable sites on CeO_2 surface (Figure 1a). The enhanced CO–Pt^{2+} peak intensity with slight peak blueshift was also observed at elevated temperatures over Pt_1/CeO_2_TS (Figure 3c). Interestingly, distinct from Pt_1/CeO_2_AT, Pt_1/CeO_2_TS shows two additional shoulder features around 2075 and 2052 cm^{-1} at temperatures ≥ 90 °C (Figure 3c). The two evolved species are not associated with either metallic Pt^0 clusters/NPs, which should show lower-wavenumber features (<2000 cm^{-1}) on extended Pt surfaces (Figure S11), or oxidized PtO_x clusters, which would show a higher-wavenumber feature (>2100 cm^{-1}).[4a,8b,12] Here, they are indexed as atop CO on the partially reduced $Pt_1^{\delta+}$ atoms with Pt_1O_{4-x} local coordinations.[10c] Recently, Wang et al., based on combined DFT calculations and ab initio atomistic thermodynamics modeling, demonstrated that monodispersed Pt^0 are thermodynamically unstable compared to bulk Pt^0, also supporting our assignment of these shoulder features to partially reduced $Pt_1^{\delta+}$ species.[22]

To evaluate the reactivities of different Pt_1 species, after CO oxidation up to 180 °C in phase-I, the catalysts were cooled down to 120 °C in the same $CO+O_2$ atmosphere followed by purging in O_2/He (phase-II of Figure 3a). As expected for Pt_1/CeO_2_AT, the CO–Pt^{2+} (2091 cm^{-1}) peak decreased very slightly after CO was discontinued (Figure 3d), consistent with the lack of low-temperature activity below 200 °C (Figure 2a). This is also consistent with the CO-DRIFTS results in previous reports.[3c,7,19] Identical experiments were also conducted on Pt_1/CeO_2_TS (Figure 3e). Notably, in contrast to CO on isolated Pt^{2+} (2096 cm^{-1}) that was only slightly removed by O_2 purging for 10 min, CO on the partially reduced $Pt_1^{\delta+}$ species (i.e., 2075 and 2052 cm^{-1} shoulder) got rapidly removed within 2 min (Figure 3e). Given that the light-off curve of CO oxidation over Pt_1/CeO_2_TS shows an onset at approximately 70 °C (Figure 2a), the excellent low-temperature activity is attributed to the reaction-induced $Pt_1^{\delta+}$ species in the reduced Pt_1O_{4-x} coordination. Careful AC-STEM investigations of the Pt_1/CeO_2_TS catalyst after the phase-I CO-DRIFTS experiments (Figure 3a) excluded the presence of Pt clusters/NPs (Figure S12), indicating that the shoulder IR features (2075 and 2052 cm^{-1}) should not be associated with Pt clusters/NPs transformed from isolated Pt^{2+}. This was further confirmed by additional CO-DRIFTS measurements that the shoulder species can be eliminated by treatment in O_2/He at 250 °C, which cannot redisperse the reduction-induced metallic Pt clusters/NPs (requiring oxidizing treatment >400 °C) (Figure S13).[8d] Synchrotron-based EXAFS analysis also confirmed the absence of Pt–Pt bonding, that is, formation of Pt/PtO_x clusters/NPs, in the spent Pt_1/CeO_2_TS catalyst after IR measurements (Figure S14). XPS of the same spent Pt_1/CeO_2_TS catalyst after IR measurement also excluded the evolution of metallic Pt^0 species after CO oxidation (Figure S15a). The partially reduced Pt states may not be able to be tracked by ex-situ XPS given that CO on the evolved Pt_1O_{4-x} species can be readily replaced by gaseous O_2. However, an increased amount of defect-related O species (15.7 %) was present on the surface of the spent Pt_1/CeO_2_TS (Figure S15b), suggesting that Pt_1O_4 was partially reduced during CO oxidation.

The DRIFTS results (Figure 3e) indicate that the reaction-induced $Pt_1^{\delta+}$ species in Pt_1/CeO_2_TS are much more reactive than as-synthesized Pt^{2+} in Pt_1/CeO_2_AT during low-temperature CO oxidation (Figure 3d), which also agree with the distinct reaction orders with respect to CO for Pt_1/CeO_2_TS (0.76) and Pt_1/CeO_2_AT (≈ 0; Figure S9). Here, both Pt_1/CeO_2_AT and Pt_1/CeO_2_TS showed an increasingly pronounced Pt_1O_4 distortion during CO oxidation at elevated temperatures (Figure 3b,c), except that the reduced $Pt_1^{\delta+}$ was only formed over Pt_1/CeO_2_TS. The formation of the partially reduced $Pt_1^{\delta+}$ species induced by the reaction is therefore ascribed to the tailored local environments (e.g., location, coordination) of Pt^{2+} single atoms produced by TS, as evidenced by the decreased Pt_1O_4 coordination symmetry (Figure 1d and Table 1) as well as the different vibrational frequency of CO–Pt^{2+} compared to those produced by AT (Figure 3b,c).

Based on above discussion, the dynamic behavior of isolated Pt^{2+} in Pt_1/CeO_2_TS during CO oxidation is depicted (Figure 4), which we postulate is a result of an asymmetric Pt_1O_4 coordination produced by TS in contrast to a highly symmetric square-planar Pt_1O_4 coordination by AT rendering over-stabilized Pt^{2+} single atoms. During CO oxidation, Pt^{2+} in Pt_1/CeO_2_TS dynamically adopts a partially reduced Pt_1O_{4-x} coordination. Due to the reduced electronic states, the evolved $Pt_1^{\delta+}$ species greatly promote CO oxidation at low temperatures, showing an exceptional activity comparable to that of clusters/NPs-containing Pt/CeO_2 catalysts (Figure S16).[3g,23] More importantly, while metallic Pt undergoes oxidation/dispersion leading to a drastic activity loss once being oxidized at 500 °C, Pt_1/CeO_2_TS retains its reactivity (Figure 2b). The dynamically interconnected charge states of isolated Pt on CeO_2 (100) surface which is phonon-assisted as

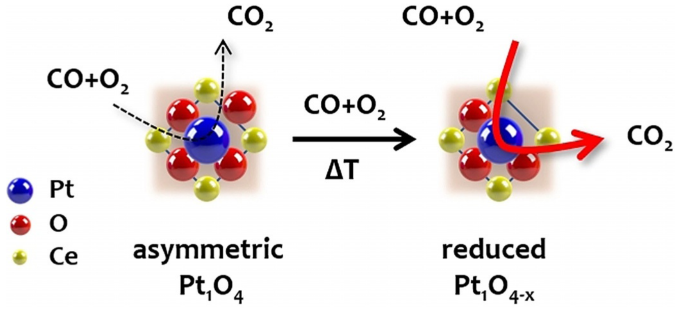

Figure 4. Proposed dynamic evolution of the local environments of isolated Pt^{2+} in Pt_1/CeO_2_TS from asymmetric (distorted) Pt_1O_4 to partially reduced Pt_1O_{4-x} for greatly enhanced low-temperature CO oxidation.

identified by combined DFT and first-principles molecular dynamics studies helps explain our experimental findings.[3h] These results here demonstrate that the thermally stable Pt_1/CeO_2 catalyst directly synthesized by a thermal-shock method is low-temperature active for CO oxidation due to the tailored local environments of isolated Pt^{2+} that is different from that achieved by atom trapping which tends to place Pt in sites that are stable but unreactive.

Conclusion

In summary, atomically dispersed Pt on CeO_2 with tailored local coordination structures and electronic states were generated by two different high-temperature synthesis approaches, namely, atom-trapping (AT) and thermal-shock (TS) synthesis. Complementary STEM, XAS, in situ DRIFTS, and CO chemisorption studies confirmed that in contrast to AT synthesis, which resulted in over-stabilized Pt^{2+} single atoms on CeO_2 with near-perfect square-planar Pt_1O_4 coordination with a high geometric symmetry, TS synthesis in an inert atmosphere stabilized isolated Pt^{2+} in an asymmetric Pt_1O_4 configuration by inducing intense surface reconstruction of CeO_2 while limiting the vapor-phase transport of PtO_2. Benefiting from such an asymmetric coordination, active $Pt_1^{\delta+}$ species in partially reduced Pt_1O_{4-x} coordination were formed during CO oxidation, leading to the greatly enhanced low-temperature activity evidenced by a decrease of T_{50} by approximately 140 °C at a high space velocity of 200 $L\,g^{-1}\,h^{-1}$. The findings here show that there is room to engineer the active sites in Pt/CeO_2 catalysts via novel synthesis methods. Comparing the behavior of Pt single atoms in different local environment provides insights into the structure-function relationship of SACs revealing dynamic site evolution as well as site-dependent reactivity that is coordination sensitive.

Acknowledgements

This work was supported by U.S. Department of Energy (DOE), Office of Science, Office of Basic Energy Sciences, Division of Chemical Sciences (grant DE-FG02-05ER15712). K.K. and C.E.G would like to acknowledge additional support from U.S. DOE, Energy Efficiency and Renewable Energy, Vehicle Technology Office for part of the IR experiments. Use of the Advanced Photon Source is supported by the U.S. Department of Energy, Office of Science, Office of Basic Energy Sciences, under Contract No. DE-AC02-06CH11357, and the Canadian Light Source and its funding partners. Use of the Stanford Synchrotron Radiation Lightsource, SLAC National Accelerator Laboratory, is supported by the U.S. Department of Energy, Office of Science, Office of Basic Energy Sciences under Contract No. DE-AC02-76SF00515. G.W. would like to acknowledge additional support from U.S. DOE, Energy Efficiency and Renewable Energy, Vehicle Technology Office. XPS measurements were performed using EMSL (grid.436923.9), a DOE Office of Science User Facility sponsored by the Office of Biological and Environmental Research. We acknowledge Dr. Fengyuan Shi at UIC for performing STEM imaging. This work made use of instruments in the Electron Microscopy Core of UIC's Research Resources Center. We also would like to thank Dr. Jiyun Hong for preparing the sample for XAS of the spent Pt_1/CeO_2_TS catalyst at SSRL.

Conflict of Interest

The authors declare no conflict of interest.

Keywords: CO oxidation · metal–support interactions · platinum · single-atom catalysis · thermal-shock synthesis

[1] a) J. Jones, H. Xiong, A. T. De La Riva, E. J. Peterson, H. Pham, S. R. Challa, G. Qi, S. Oh, M. H. Wiebenga, X. I. P. Hernández, *Science* **2016**, *353*, 150–154; b) B. Qiao, A. Wang, X. Yang, L. F. Allard, Z. Jiang, Y. Cui, J. Liu, J. Li, T. Zhang, *Nat. Chem.* **2011**, *3*, 634–641; c) J. Shan, M. Li, L. F. Allard, S. Lee, M. Flytzani-Stephanopoulos, *Nature* **2017**, *551*, 605–608; d) L. Cao, W. Liu, Q. Luo, R. Yin, B. Wang, J. Weissenrieder, M. Soldemo, H. Yan, Y. Lin, Z. Sun, C. Ma, W. Zhang, S. Chen, H. Wang, Q. Guan, T. Yao, S. Wei, J. Yang, J. Lu, *Nature* **2019**, *565*, 631–635; e) B.-H. Lee, S. Park, M. Kim, A. K. Sinha, S. C. Lee, E. Jung, W. J. Chang, K.-S. Lee, J. H. Kim, S.-P. Cho, *Nat. Mater.* **2019**, *18*, 620–626; f) C. Zhu, S. Fu, Q. Shi, D. Du, Y. Lin, *Angew. Chem. Int. Ed.* **2017**, *56*, 13944–13960; *Angew. Chem.* **2017**, *129*, 14132–14148.

[2] a) M. Cargnello, V. V. Doan-Nguyen, T. R. Gordon, R. E. Diaz, E. A. Stach, R. J. Gorte, P. Fornasiero, C. B. Murray, *Science* **2013**, *341*, 771–773; b) C. K. Lambert, *Nat. Catal.* **2019**, *2*, 554–557; c) A. Beniya, S. Higashi, *Nat. Catal.* **2019**, *2*, 590–602; d) A. K. Datye, M. Votsmeier, *Nat. Mater.* **2021**, *20*, 1049–1059.

[3] a) D. Kunwar, S. Zhou, A. De La Riva, E. Peterson, H. Xiong, X. I. Pereira Hernandez, S. C. Purdy, R. ter Veen, H. H. Brongersma, J. T. Miller, H. Hashiguchi, L. Kovarik, S. Lin, H. Guo, Y. Wang, A. Datye, *ACS Catal.* **2019**, *9*, 3978–3990; b) F. Dvořák, M. F. Camellone, A. Tovt, N.-D. Tran, F. R. Negreiros, M. Vorokhta, T. Skála, I. Matolínová, J. Mysliveček, V. Matolín, *Nat. Commun.* **2016**, *7*, 10801; c) L. Nie, D. Mei, H. Xiong, B. Peng, Z. Ren, X. I. P. Hernandez, A. De La Riva, M. Wang, M. H. Engelhard, L. Kovarik, *Science* **2017**, *358*, 1419–1423; d) G. Ferré, M. Aouine, F. Bosselet, L. Burel, F. J. Cadete Santos Aires, C. Geantet, S. Ntais, F. Maurer, M. Casapu, J. D. Grunwaldt, T. Epicier, S. Loridant, P. Vernoux, *Catal. Sci. Technol.* **2020**, *10*, 3904–3917; e) F. Maurer, J. Jelic, J. Wang, A.

Gänzler, P. Dolcet, C. Wöll, Y. Wang, F. Studt, M. Casapu, J.-D. Grunwaldt, *Nat. Catal.* **2020**, *3*, 824 – 833; f) A. J. Therrien, A. J. Hensley, M. D. Marcinkowski, R. Zhang, F. R. Lucci, B. Coughlin, A. C. Schilling, J.-S. McEwen, E. C. H. Sykes, *Nat. Catal.* **2018**, *1*, 192 – 198; g) J. Resasco, L. DeRita, S. Dai, J. P. Chada, M. Xu, X. Yan, J. Finzel, S. Hanukovich, A. S. Hoffman, G. W. Graham, S. R. Bare, X. Pan, P. Christopher, *J. Am. Chem. Soc.* **2020**, *142*, 169 – 184; h) N. Daelman, M. Capdevila-Cortada, N. López, *Nat. Mater.* **2019**, *18*, 1215 – 1221.

[4] a) P. Xie, T. Pu, A. Nie, S. Hwang, S. C. Purdy, W. Yu, D. Su, J. T. Miller, C. Wang, *ACS Catal.* **2018**, *8*, 4044 – 4048; b) R. Lang, W. Xi, J.-C. Liu, Y.-T. Cui, T. Li, A. F. Lee, F. Chen, Y. Chen, L. Li, L. Li, J. Lin, S. Miao, X. Liu, A.-Q. Wang, X. Wang, J. Luo, B. Qiao, J. Li, T. Zhang, *Nat. Commun.* **2019**, *10*, 234; c) D. Yan, J. Chen, H.-P. Jia, *Angew. Chem. Int. Ed.* **2020**, *59*, 13562 – 13567; *Angew. Chem.* **2020**, *132*, 13664 – 13669.

[5] a) H. A. Aleksandrov, K. M. Neyman, G. N. Vayssilov, *Phys. Chem. Chem. Phys.* **2015**, *17*, 14551 – 14560; b) Y. Lykhach, A. Figueroba, M. F. Camellone, A. Neitzel, T. Skála, F. R. Negreiros, M. Vorokhta, N. Tsud, K. C. Prince, S. Fabris, K. M. Neyman, V. Matolín, J. Libuda, *Phys. Chem. Chem. Phys.* **2016**, *18*, 7672 – 7679.

[6] a) A. Bruix, Y. Lykhach, I. Matolínová, A. Neitzel, T. Skála, N. Tsud, M. Vorokhta, V. Stetsovych, K. Ševčíková, J. Mysliveček, *Angew. Chem. Int. Ed.* **2014**, *53*, 10525 – 10530; *Angew. Chem.* **2014**, *126*, 10693 – 10698; b) A. Neitzel, Y. Lykhach, T. Skála, N. Tsud, M. Vorokhta, D. Mazur, K. C. Prince, V. Matolín, J. Libuda, *Phys. Chem. Chem. Phys.* **2014**, *16*, 24747 – 24754; c) Y. Tang, Y.-G. Wang, J. Li, *J. Phys. Chem. C* **2017**, *121*, 11281 – 11289.

[7] X. I. Pereira-Hernández, A. De La Riva, V. Muravev, D. Kunwar, H. Xiong, B. Sudduth, M. Engelhard, L. Kovarik, E. J. Hensen, Y. Wang, *Nat. Commun.* **2019**, *10*, 1358.

[8] a) X. Liu, S. Jia, M. Yang, Y. Tang, Y. Wen, S. Chu, J. Wang, B. Shan, R. Chen, *Nat. Commun.* **2020**, *11*, 4240; b) H. Wang, J.-X. Liu, L. F. Allard, S. Lee, J. Liu, H. Li, J. Wang, J. Wang, S. H. Oh, W. Li, *Nat. Commun.* **2019**, *10*, 1 – 12; c) Y. Lu, C. Thompson, D. Kunwar, A. Datye, A. M. Karim, *ChemCatChem* **2020**, *12*, 1726 – 1733; d) A. M. Gänzler, M. Casapu, P. Vernoux, S. Loridant, F. J. Cadete Santos Aires, T. Epicier, B. Betz, R. Hoyer, J. D. Grunwaldt, *Angew. Chem. Int. Ed.* **2017**, *56*, 13078 – 13082; *Angew. Chem.* **2017**, *129*, 13258 – 13262.

[9] a) L. DeRita, S. Dai, K. Lopez-Zepeda, N. Pham, G. W. Graham, X. Pan, P. Christopher, *J. Am. Chem. Soc.* **2017**, *139*, 14150 – 14165; b) H. V. Thang, G. Pacchioni, L. DeRita, P. Christopher, *J. Catal.* **2018**, *367*, 104 – 114.

[10] a) M. J. Kale, P. Christopher, *ACS Catal.* **2016**, *6*, 5599 – 5609; b) K. Alexopoulos, Y. Wang, D. G. Vlachos, *ACS Catal.* **2019**, *9*, 5002 – 5010; c) L. DeRita, J. Resasco, S. Dai, A. Boubnov, H. V. Thang, A. S. Hoffman, I. Ro, G. W. Graham, S. R. Bare, G. Pacchioni, *Nat. Mater.* **2019**, *18*, 746 – 751; d) Y. Tang, C. Asokan, M. Xu, G. W. Graham, X. Pan, P. Christopher, J. Li, P. Sautet, *Nat. Commun.* **2019**, *10*, 1 – 10; e) D. Jiang, G. Wan, C. E. Garcia Vargas, L. Li, X. I. Pereira Hernandez, C. Wang, Y. Wang, *ACS Catal.* **2020**, *10*, 11356 – 11364; f) T. Avanesian, S. Dai, M. J. Kale, G. W. Graham, X. Pan, P. Christopher, *J. Am. Chem. Soc.* **2017**, *139*, 4551 – 4558; g) L. Liu, D. M. Meira, R. Arenal, P. Concepcion, A. V. Puga, A. Corma, *ACS Catal.* **2019**, *9*, 10626 – 10639.

[11] a) Y. Yao, Z. Huang, P. Xie, S. D. Lacey, R. J. Jacob, H. Xie, F. Chen, A. Nie, T. Pu, M. Rehwoldt, D. Yu, M. R. Zachariah, C. Wang, R. Shahbazian-Yassar, J. Li, L. Hu, *Science* **2018**, *359*, 1489 – 1494; b) Y. Yao, Z. Huang, P. Xie, L. Wu, L. Ma, T. Li, Z. Pang, M. Jiao, Z. Liang, J. Gao, Y. He, D. J. Kline, M. R. Zachariah, C. Wang, J. Lu, T. Wu, T. Li, C. Wang, R. Shahbazian-Yassar, L. Hu, *Nat. Nanotechnol.* **2019**, *14*, 851 – 857; c) Y. Yao, Z. Huang, T. Li, H. Wang, Y. Liu, H. S. Stein, Y. Mao, J. Gao, M. Jiao, Q. Dong, J. Dai, P. Xie, H. Xie, S. D. Lacey, I. Takeuchi, J. M. Gregoire, R. Jiang, C. Wang, A. D. Taylor, R. Shahbazian-Yassar, L. Hu, *Proc. Natl. Acad. Sci. USA* **2020**, *117*, 6316 – 6322.

[12] M. Kottwitz, Y. Li, R. M. Palomino, Z. Liu, G. Wang, Q. Wu, J. Huang, J. Timoshenko, S. D. Senanayake, M. Balasubramanian, D. Lu, R. G. Nuzzo, A. I. Frenkel, *ACS Catal.* **2019**, *9*, 8738 – 8748.

[13] A. Ankudinov, J. Rehr, J. Low, S. Bare, *Top. Catal.* **2002**, *18*, 3 – 7.

[14] A. Ankudinov, J. Rehr, J. J. Low, S. R. Bare, *J. Chem. Phys.* **2002**, *116*, 1911 – 1919.

[15] a) C. Yang, X. Yu, S. Heißler, A. Nefedov, S. Colussi, J. Llorca, A. Trovarelli, Y. Wang, C. Wöll, *Angew. Chem. Int. Ed.* **2017**, *56*, 375 – 379; *Angew. Chem.* **2017**, *129*, 382 – 387; b) C. Yang, M. Capdevila-Cortada, C. Dong, Y. Zhou, J. Wang, X. Yu, A. Nefedov, S. Heißler, N. López, W. Shen, C. Wöll, Y. Wang, *J. Phys. Chem. Lett.* **2020**, *11*, 7925 – 7931.

[16] a) C. Yang, X. Yu, S. Heissler, P. G. Weidler, A. Nefedov, Y. Wang, C. Woell, T. Kropp, J. Paier, J. Sauer, *Angew. Chem. Int. Ed.* **2017**, *56*, 16399 – 16404; *Angew. Chem.* **2017**, *129*, 16618 – 16623; b) D. Jiang, W. Wang, L. Zhang, Y. Zheng, Z. Wang, *ACS Catal.* **2015**, *5*, 4851 – 4858; c) F. Polo-Garzon, Z. Bao, X. Zhang, W. Huang, Z. Wu, *ACS Catal.* **2019**, *9*, 5692 – 5707; d) G. Spezzati, A. Benavidez, A. T. De La Riva, Y. Su, J. P. Hofmann, S. Asahina, E. J. Olivier, J. H. Neethling, J. T. Miller, A. K. Datye, E. J. M. Hensen, *Appl. Catal. B* **2019**, *243*, 36 – 46.

[17] a) D. Jiang, W. Wang, L. Zhang, R. Qiu, S. Sun, Y. Zheng, *Appl. Catal. B* **2015**, *165*, 399 – 407; b) D. Jiang, W. Wang, Y. Zheng, L. Zhang, *Appl. Catal. B* **2016**, *191*, 86 – 93; c) D. Jiang, W. Wang, E. Gao, S. Sun, L. Zhang, *Chem. Commun.* **2014**, *50*, 2005 – 2007.

[18] a) D. Daniel, *J. Phys. Chem.* **1988**, *92*, 3891 – 3899; b) J. Ke, W. Zhu, Y. Jiang, R. Si, Y.-J. Wang, S.-C. Li, C. Jin, H. Liu, W.-G. Song, C.-H. Yan, *ACS Catal.* **2015**, *5*, 5164 – 5173; c) C. Lentz, S. P. Jand, J. Melke, C. Roth, P. Kaghazchi, *J. Mol. Catal. A Chem.* **2017**, *426*, 1 – 9; d) Y. Lykhach, A. Bruix, S. Fabris, V. Potin, I. Matolínová, V. Matolín, J. Libuda, K. M. Neyman, *Catal. Sci. Technol.* **2017**, *7*, 4315 – 4345.

[19] K. Ding, A. Gulec, A. M. Johnson, N. M. Schweitzer, G. D. Stucky, L. D. Marks, P. C. Stair, *Science* **2015**, *350*, 189 – 192.

[20] H. A. Aleksandrov, K. M. Neyman, K. I. Hadjiivanov, G. N. Vayssilov, *Phys. Chem. Chem. Phys.* **2016**, *18*, 22108 – 22121.

[21] M. A. Newton, C. Belver-Coldeira, A. Martínez-Arias, M. Fernández-García, *Nat. Mater.* **2007**, *6*, 528 – 532.

[22] X. Wang, J. A. van Bokhoven, D. Palagin, *Phys. Chem. Chem. Phys.* **2020**, *22*, 28 – 38.

[23] K. An, S. Alayoglu, N. Musselwhite, S. Plamthottam, G. Melaet, A. E. Lindeman, G. A. Somorjai, *J. Am. Chem. Soc.* **2013**, *135*, 16689 – 16696.

Manuscript received: June 28, 2021
Accepted manuscript online: August 3, 2021
Version of record online: September 7, 2021

